Journal of Hydraulic Research

ISSN: (Print) (Online) Journal homepage: www.tandfonline.com/journals/tjhr20

Experimental and numerical investigation of a small scale storm sewer geyser

Pratik Mahyawansi, Sumit R. Zanje, Abbas Sharifi, Dwayne McDaniel & Arturo S. Leon

To cite this article: Pratik Mahyawansi, Sumit R. Zanje, Abbas Sharifi, Dwayne McDaniel & Arturo S. Leon (2024) Experimental and numerical investigation of a small scale storm sewer geyser, Journal of Hydraulic Research, 62:1, 25-38, DOI: 10.1080/00221686.2024.2305353

To link to this article: https://doi.org/10.1080/00221686.2024.2305353

Published online: 15 Feb 2024.

JOURNAL OF HYDRAULIC RESEARCH
2024, VOL. 62, NO. 1, 25–38
https://doi.org/10.1080/00221686.2024.2305353

International Association for Hydro-Environment Engineering and Research
Hosted by Spain Water and IWHR, China

Taylor & Francis
Taylor & Francis Group

RESEARCH PAPER

Experimental and numerical investigation of a small scale storm sewer geyser

Pratik Mahyawansi [a], Sumit R. Zanje[b], Abbas Sharifi[b], Dwayne McDaniel[a] and Arturo S. Leon[b]

[a]Department of Mechanical and Materials Engineering, Florida International University, Miami, FL, USA; [b]Department of Civil and Environmental Engineering, Florida International University, Miami, FL, USA

ABSTRACT

The violent nature of storm sewer geysers has been puzzling researchers worldwide for a very long time. This paper investigates the geyser simulation methodology using a small-scale set-up, where important flow structures such as slugs, eruption patterns, and pressure oscillations are compared with experimental results to test the fidelity of the numerical modelling. In this exercise, a geyser-like process is produced using a continuous insertion of air in the horizontal pipe. The established methodology is used to simulate the hypothesized scenario of a finite trapped air pocket in the relatively longer pipe system. A geyser produced from a finitely trapped air pocket shows a different eruption mechanism compared to those found in previous studies. First, no slug is observed in the horizontal pipe, resulting in continuous air release. Second, the interface continuously atomizes in the vertical pipe, creating a churn-slug flow that produces a large number of small eruptions.

ARTICLE HISTORY
Received 16 March 2023
Accepted 7 January 2024
Open for discussion until
1 August 2024

KEYWORDS
Geyser; LES; multiphase flow; PIV; slug flow; VOF

1. Introduction

A storm sewer geyser is a highly unsteady phenomenon where an air–water mixture violently erupts from the sewer system. The eruption has enough strength to eject the storm sewer metal lid, which weighs approximately 120 kg. Once the lid is ejected, the chain of eruptions may reach heights exceeding 30 m. However, the hydrostatic pressure just before the eruption is low and cannot justify the violent eruptions. In the event of heavy rain, the flow in the sewer tunnel transforms from stratified to pressurized flow, during which the air in the tunnel gets trapped due to poor venting. This trapped air moves with the flow and is released through the vertical pipe. The release of pressurized air initiates a sequence of events that may lead to a violent geyser. Wright et al. (2011) have recorded a geyser event in Minnesota where they showed pressure in the system gradually increases, and after some time, it drops abruptly during the eruption that lasts around 15 s. After the first eruption, the pipe junction is depressurized, and pressure again increases rapidly and causes the next eruption; this process continues until all the trapped air in the system is removed. The major challenge in geyser research is its large scale, which makes it very challenging to conduct systematic experiments. Also, the simulation strategy is not fully established and cannot confidently predict geyser phenomena. The large uncertainties in the predictions limit engineers and designers from developing retrofits that can effectively suppress the storm sewer geyser.

Numerical modelling of storm sewer geysers is required to accurately predict geyser characteristics such as maximum eruption velocity, maximum eruption height, and the number of eruptions. This will aid engineers in designing a retrofit that can effectively reduce geyser intensity. The large-scale system poses a major challenge for conducting experimental measurements of flow structures to compare with numerical studies for validation. Therefore, this paper focuses on a small-scale set-up to generate the experimental data required for computational fluid dynamics (CFD) validations using a state-of-the-art large eddy simulation (LES) model. Another challenge in the simulations is determining the boundary conditions and air insertion methodology. The second part of this paper studies geysers that are spontaneously produced using a trapped air pocket. This approach will allow researchers to simulate geysers under various operating conditions and identify violent geysers within a given system.

2. Current state-of-art

In this section, some of the major contributions to storm sewer geyser research are discussed. A few fundamental benchmark cases for the simulation of the gas–liquid multiphase flow problem are then discussed.

The research on storm sewer geysers has been challenging due to their extremely large scales. Guo and Song (1990) modelled the surging phenomenon in the TARP (Tunnel and Reservoir Plan) Phase-1 Mainstream System, and the result showed how the surging in the system could lead to spillage at some stations. However, the model could not show the actual geyser, which is violent and more than just

CONTACT Pratik Mahyawansi pmahy002@fiu.edu

water spillage. Muller et al. (2017) investigated geyser eruptions in a large-diameter pipe system using experiments and simulations. The simulations are carried out using the OpenFOAM solver with k–ϵ turbulence mode. The results are validated against the normalized pressure fluctuations and normalized interface location. The simulated pressure fluctuations are found to be overpredicted in magnitude and frequency. This is probably due to the poor modelling of the influence of turbulence on interface localization. Leon (2019) has conducted several experiments and identified the generation of slugs, which act as a precursor to geysers and result in multiple eruptions. Vasconcelos and Wright (2011) studied geysers experimentally using pressurized air pockets which results in spillage and harmonic oscillation of water in the vertical pipe. Qian et al. (2020) investigated geyser and mitigation strategies using experiments and numerical approaches. The study showed the inflow control method is superior to the orifice plate method to mitigate the geyser. Zanje et al. (2022) showed numerically the geyser eruptions generated with a non-zero pressure gradient and appropriate boundary conditions. However, the flow structures observed in the simulations are not compared with experimental results, which limits the application of the methodology in quantifying the geyser severity.

The occurrence of violent geysers in the storm sewer system is attributed to various factors, including the exsolution of gases, the arrival of trapped air pockets from upstream (Leon, 2019), and the arrival of trapped air pockets from the downstream (Wright et al., 2011). Among these factors, upstream trapped air pockets are widely studied to explore the violent geysers in storm sewers. Vasconcelos and Wright (2006) investigated the role of inflow rate and geometry on the production of air pockets during the transition of gravity flow to pressurized flow. The study speculates on the possibility of large air pockets forming in the storm sewer tunnel due to the rapid filling. Numerous experimental studies have been conducted, but detailed flow measurements and visualizations, such as slug velocity, have not been reported. This is primarily because these experiments are generally conducted outdoors and are not conducive to the use of flow diagnostic instruments, owing to the large size of the system. Therefore, numerical modelling is important for geyser studies. However, this modelling methodology requires thorough validation. Small-scale indoor experiments enable detailed flow measurements using PIV and high-speed flow visualization. While the small-scale experimental study may not fully replicate real-world scenarios, it does share similarities with geyser physics, including slug flow, eruption patterns, and interface dynamics near the junction. Consequently, these experimental cases can be used to evaluate the accuracy of the numerical methodology and quantify prediction errors.

Modelling the impact of turbulence on interface localization and deformation is a major challenge in gas–liquid multiphase flow simulation. Lakehal et al. (2003) conducted a DNS (direct numerical simulation) study of turbulence in a stratified flow of air and water for a low Reynolds number of 171. The study found the turbulence intensity at the interface is similar to that of the near-wall boundary. Most importantly, the study shows that the presence of an interface does not significantly impact the quasi-streamwise vortices. Mortazavi et al. (2016) carried out a DNS study of the hydraulic jump phenomenon where the interface is tracked using a hybrid Lagrangian–Eulerian scheme (HyLEM). The tracking scheme is coupled with level-set equations to represent the interface accurately. Pavlidis et al. (2014) studied slug flow in a horizontal pipe using a higher-order accurate compressive advection method with LES. The grid refinement of 18 cells across the pipe diameters is found to be sufficient for capturing slugging for the structured grid. The methodology also promises to eliminate spurious velocities in the case of unstructured grids, which are not generally used for multiphase flow simulation. The methodology of LES for multiphase flow has been explored by many workers, with various mechanisms to track the interface. Lakehal (2018) reviewed some of the important modelling strategies and developed a unified approach called ARM (All-Regime Multiphase flow model) which can deal with both the resolved large interface scale and unresolved dispersed phases. Hirt and Nichols (1981) proposed the VOF (volume-of-fluid) method to track the interface in an Eulerian mesh. So et al. (2012) proposed sharpening the VOF interface for a compressible flow. The scheme estimates the diffusion of the interface and applies a correction to the interface by solving additional corrector equations after each flow time step. In a large-scale study, Gupta et al. (2015) studied the performance of VOF with anti-diffusion in Ansys-Fluent for various multiphase problems with the structured and unstructured grid. The performance of the anti-diffusion scheme shows promising results in interface diffusion reductions.

Previous numerical studies qualitatively compare pressure plots; however, one-on-one comparisons are not widely reported. Additionally, detailed comparisons of important flow structures, such as slugs and eruption patterns, are lacking. The rest of the paper is organized as follows: first, the development of a simulation methodology using the LES model with an anti-diffusion VOF scheme, which has been proven effective by previous researchers in dealing with unsteady multiphase flow problems. Second, inspired by Qian et al. (2020), the paper proposes to investigate geysers produced by a finite air pocket rather than air injection in the system, but with pressure boundary conditions at all the inlets and outlets. The trapped

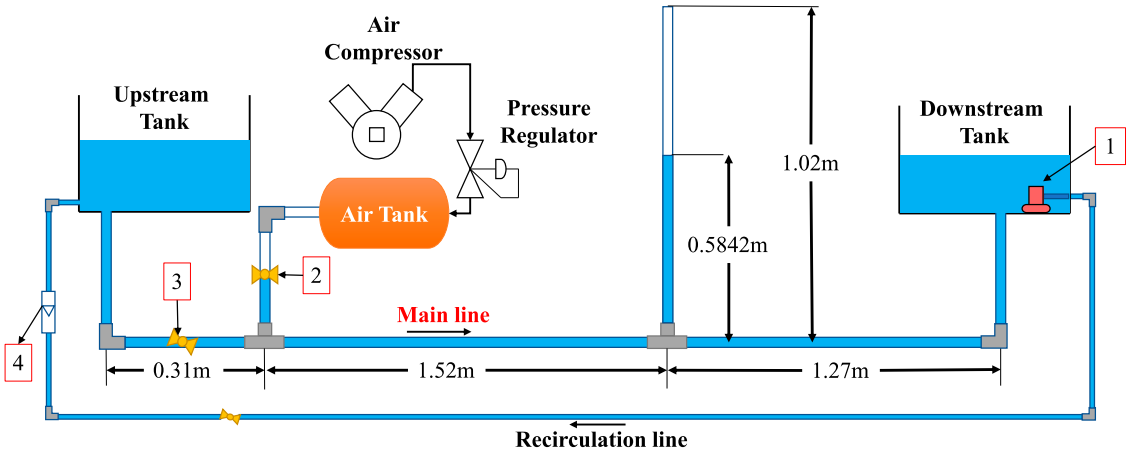

Figure 1. Experimental set-up for small-scale geyser with main line pipe diameter of 0.0254 m. Number 1 is a submersible pump; number 2 is a ball valve separating the air tank from the main line; number 3 is a ball valve partially open to prevent air from moving upstream, and number 4 is a rotameter.

air pocket situation is a momentary occurrence during the rapid filling process, as shown by Vasconcelos and Wright (2006) in a small-scale set-up. In the current numerical study, this air pocket is patched into a steady flow field to replicate the momentary air pocket.

3. Experimental set-up

A flow circuit is constructed using a PVC pipe of nominal diameter 0.0254 m, as shown in Figure 1. A vertical pipe is placed at a location that ensures the flow is fully developed. The flow is recirculated using a submersible pump through a rigid PVC pipe of diameter 0.0127 mA rotameter is connected to the re-circulation line to measure the flow rate. As water is pumped to the left tank, the water flows from left to right in the main flow line due to the difference in head. Depending on the flow rate, the system will take a few minutes to reach a steady state, i.e. the water head difference in the tank is fixed. An air tank, connected to the main line, supplies air at elevated pressure to the system. A ball valve is placed between the air tank and the main line to isolate the two systems. A reciprocating compressor is used to pressurize the tank to a pressure equal to the hydrostatic pressure, just enough to allow smooth injection of air in the system.

Once the flow in the mainline reaches steady state, the ball valve is opened, and air enters the horizontal pipe. The pressure in the tank is maintained just enough to allow the smooth insertion of air. As the air pocket moves in both directions, a second ball valve in the horizontal pipe is kept partially open to prevent upstream air movement. The position of the ball valve's handle is determined through trial and error and remains fixed for the entire experiment. In the downstream, the air pocket moves slowly with a larger volume at the leading end. The interaction of this air pocket with the vertical pipe may ultimately lead to the formation of a geyser. The entire event is unsteady and consists of some important rapid stages such as eruptions, production of slugs in the horizontal pipe, and re-accumulation of water at the junction. This event is recorded using a high-speed camera, with the flow seeded with 50-μm-sized polyamide glass spheres and illuminated using a continuous wave laser sheet. The PIV (particle image velocimetry) calculation for each event is performed using the MATLAB PIV toolbox by Thielicke and Sonntag (2021). As this involves multiphase flow, the PIV calculations are reliable only for unmixed (stratified flow), as mixed flow can lead to light refraction and increased uncertainty. The PIV methodology has been successfully tested on the same set-up for a single-phase flow by Mahyawansi, Zange, et al. (2022).

4. CFD methodology

A three-dimensional CFD domain is designed using the dimensions of the experimental set-up to simulate a geyser. The CFD set-up is shown in Figure 2. The water tanks are not modelled in the simulation due to computational limitations, and the tanks' role in absorbing high-frequency pressure fluctuations is ignored in the present study. Two types of mesh are considered: (1) a polyhedra mesh generated using Ansys-Fluent mesher (Ansys, 2022) with two different sizes, 1.4 and 2.7 million, and (2) a cut cell mesh generated using an Ansys mesher with three different sizes, 0.3, 0.5 and 1.2 million cells, as shown in Figure 3. Three refinement levels are considered in the case of the cut cell mesh: coarse mesh, medium-refine mesh and refined mesh. In the medium-refine, a body of influence is added in the eruption region, and in the refined mesh, in addition to the body of influence, cells in the pipe are further refined. In the polyhedral mesh, the refinement is simply adjusted by increasing cells per gap. In all cases, inflation layers with five layers are placed on the pipe wall for near-wall treatment.

In the solver set-up, an unsteady pressure-based solver with gravity is employed, and a VOF multiphase

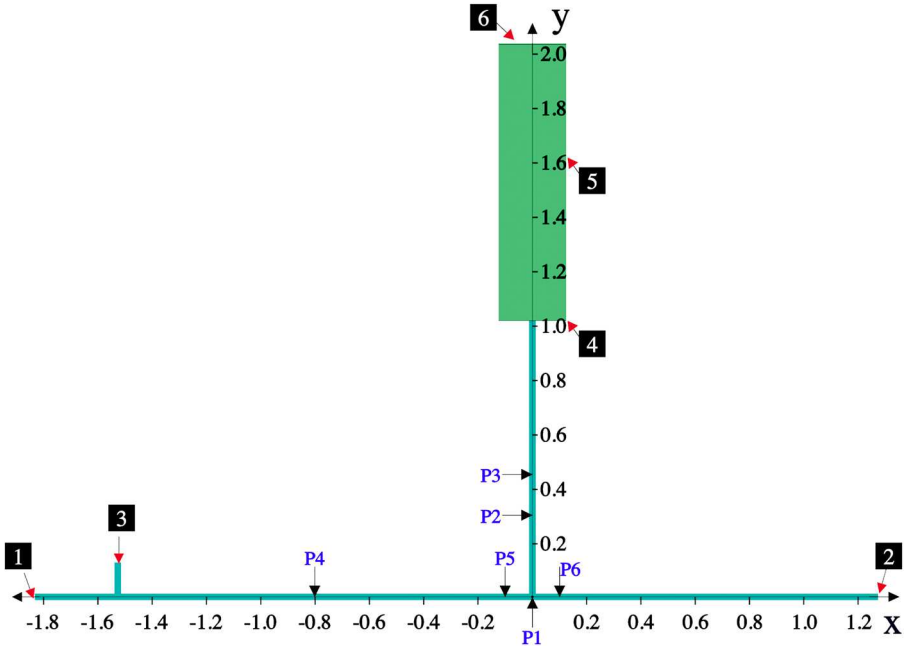

Figure 2. CFD domain for a 0.0254 m diameter pipe with boundary numbering. The locations of the probes on the central lines are as follows: P1 is at the origin, and P2 and P3 are at $y = 0.3$ m and $y = 0.45$ m, respectively. P4, P5 and P6 are positioned at $x = -0.8$ m, $x = -0.1$ m and $x = 0.1$ m, respectively.

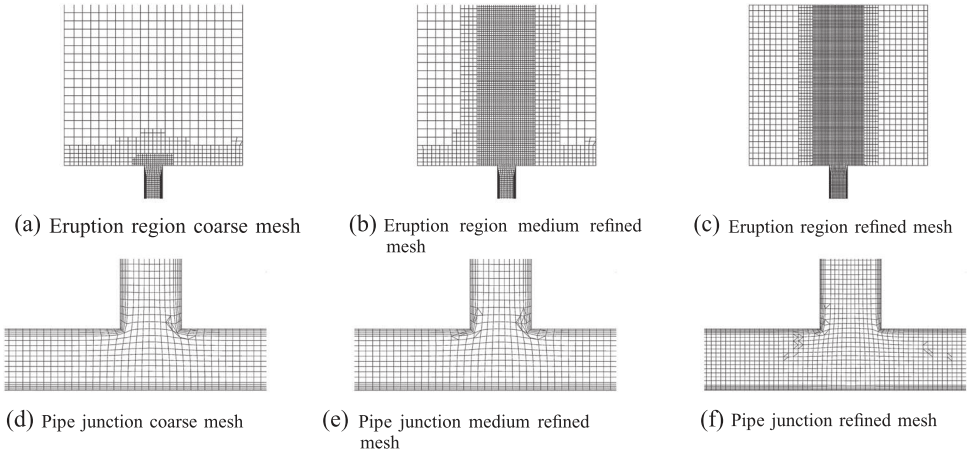

Figure 3. Cutcell mesh on the eruption region and pipe junction for coarse (0.3 M), medium-refine (0.5 M), and refine grid (1.2 M).

flow option is selected to track the air–water interface. The interface is tracked using a sharp implicit scheme. The VOF model is coupled with an anti-diffusion model to restrict interface diffusion. Since the pipe diameter is small, surface tension is also considered. The air is treated as a compressible ideal gas, and water as a compressible liquid. All other properties of air and water are kept constant at standard values. The LES model is used for resolving large turbulent structures of the flow with the Smagorinsky subgrid model, which models the filtered stresses. Inlet and outlet boundaries are treated as total pressure boundaries, as the pressure in the tank remains constant during the geyser. The pressure head difference across the pipe is maintained to match the flow rate measured by the rotameter. Detailed boundary conditions are shown in Table 1.

Table 1. Boundary conditions used for all the simulations with the air inlet.

Boundary	Purpose	Boundary type	Value (Pa)	Water volume fraction
1	Water inlet	Pressure inlet	$\rho_2 g(0.586 - y)$	1
2	Water outlet	Pressure outlet	$\rho_2 g(0.584 - y)$	1
3	Air supply	Pressure inlet	5700	0
4	Ambient	Pressure outlet	0	0
5	Ambient	Pressure outlet	$\rho_1 g(1.02 - y)$	0
6	Ambient	Pressure outlet	$\rho_1 g(1.02 - y)$	0

Note: Here ρ_2, ρ_1, g and y are the water density, air density, acceleration due to gravity, and y-coordinate, respectively.

All simulations are carried out in two stages. In the first stage, simple water flow is allowed to reach a steady state where all pressure–velocity fluctuation reaches zero. In this stage air-inlet boundary is treated as a wall, similar to the experimental set-up. SST (shear stress transport) k–ω is used for this stage with auto time-stepping. In the second stage, the air-inlet boundary is now treated as a pressure inlet with air, and the LES model is switched ON. The coupled solver is employed with second-order discretization for density, energy and pressure. Momentum is discretized using a bounded central difference scheme. The volume fraction equation is discretized using a modified HRIC (high-resolution interface capturing) scheme. An implicit bounded second-order scheme is used for temporal discretization as recommended for LES. Adaptive time stepping is set to maintain Courant number 5 with a time-stepping range of 1e−3 to 1e−5 s. The time step fluctuates around 1e−4 s. The second stage is simulated for at least 25 s to realize the repetitive nature of the eruptions.

The pressure and velocity are monitored at all the probe locations mentioned in Figure 2 at each time step. Water volume fraction and velocity contours are recorded at a rate of 100 Hz to capture all the unsteady details. Additionally, iso-surfaces of water volume fraction at 0.5 are recorded at the same rate to visualize the eruptions. These iso-surfaces are rendered in Blender-Online-Community (2020) for better visualization.

4.1. Governing equations

In two-phase flow, the continuity equation (Equation (1)) is expressed in terms of the volume fraction of the secondary phase:

$$\frac{\partial(\alpha_2\rho_2)}{\partial t} + \nabla.(\alpha_2\rho_2 V) = 0 \tag{1}$$

Here, α_2 is the secondary phase (water) volume fraction, and its value ranges from 0 to 1. The primary phase (air) volume fraction will be $\alpha_1 = 1 - \alpha_2$. The mixture material properties such as density (ρ) and dynamic viscosity (μ) are calculated using weighted phase volume fractions as shown in Equation (2). Subscripts 1 and 2 represent air and water, respectively. Equations (3) and (4) show the momentum and energy equations shared among phases with the combined material properties. Here $\boldsymbol{V}$, $\boldsymbol{g}$, $\boldsymbol{F}$ and $\mathbf{I}$ are flow velocity, acceleration due to gravity, surface tension force and identity tensor, respectively. Also, E and T are the mass-weighted average energy and temperature, respectively. Similarly, turbulent kinetic energy and dissipations are also shared among phases. k_{eff} is the effective thermal conductivity shared among phases similar to other properties. In the case of LES, all the equations will be Favre-filtered for compressible flow:

$$\rho = \alpha_2\rho_2 + (1-\alpha_2)\rho_1, \quad \mu = \alpha_2\mu_2 + (1-\alpha_2)\mu_1 \tag{2}$$

$$\begin{aligned}&\frac{\partial(\rho V)}{\partial t} + \nabla\cdot(\rho VV)\\ &= -\nabla p + \nabla\cdot(\mu(\nabla V + (\nabla V)^{\top})\\ &\quad - \frac{2}{3}\mu(\nabla\cdot V)\mathbf{I}) + \rho g + F\end{aligned} \tag{3}$$

$$\frac{\partial(\rho E)}{\partial t} + \nabla\cdot(V(\rho E + p)) = \nabla\cdot(k_{eff}\nabla T) \tag{4}$$

In the case of LES, the residue stress term additionally appears in the momentum equation, which requires separate modelling known as subgrid-scale models. The residue stress ($\boldsymbol{\tau_{ij}}$) can be presented in Equation (5). Here μ_t and $\bar{\mathbf{S}}_{\mathbf{ij}}$ are the eddy-viscosity and rate-of-strain tensor for the resolved scale, respectively:

$$\boldsymbol{\tau_{ij}} = -2\mu_t\bar{\mathbf{S}}_{\mathbf{ij}} \tag{5}$$

In the Smagorinsky model, μ_t is predicted by Equation (6). Here L_s is the mixing length estimated using Equation (7) where k, d, C_s and Δ are the von Kármán constant, closest wall distance, Smagorinsky constant and local grid scale, respectively:

$$\mu_t = \rho L_s^2\sqrt{2\bar{\mathbf{S}}_{\mathbf{ij}}\bar{\mathbf{S}}_{\mathbf{ij}}} \tag{6}$$

$$L_s = \min(kd, C_s\Delta) \tag{7}$$

4.2. Grid independent study

The simulation with the polyhedral mesh produced initial spillage but failed to develop subsequent eruptions. After the spillage, the flow in the horizontal pipe seems to be frozen, with the interface locked in one position and the mixture in the vertical pipe reaching equilibrium. The results are far from the experimental observations; hence, the polyhedral results are not discussed further in this article. In contrast, the cut cell meshes successfully replicated experimental observations in terms of slug production, eruption height, and the nature of pressure fluctuations. However, detailed images of the slug movement show that the most refined cut cell mesh closely matches the experimental images.

The continuous air supply produces a repeating geyser-like process. This process comprises Taylor bubble rise, spillage and eruptions, formation of slugs, and harmonic oscillation of the system. The entire process takes approximately 9.5 s. Experimental images were captured after 500 s to eliminate any potential human error resulting from manually opening the ball valve for air insertion. These images were then compared with numerical simulations that ran for 50 s. The simulations were halted once the repeating pattern of the process was confirmed.

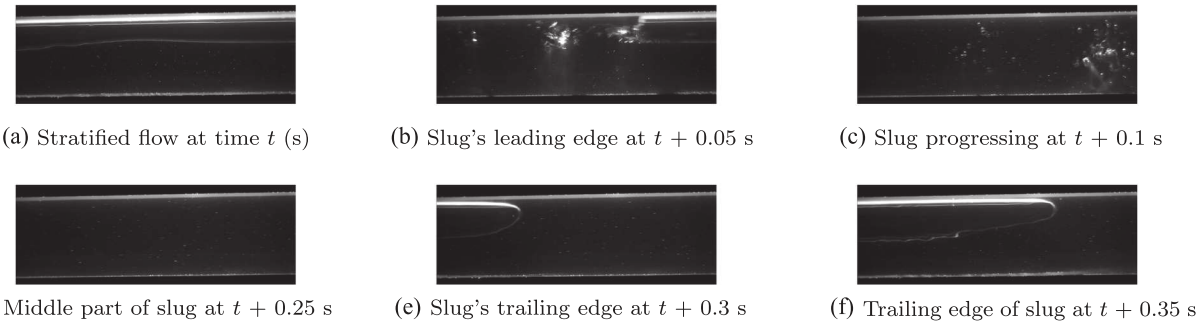

(a) Stratified flow at time t (s) (b) Slug's leading edge at $t + 0.05$ s (c) Slug progressing at $t + 0.1$ s

(d) Middle part of slug at $t + 0.25$ s (e) Slug's trailing edge at $t + 0.3$ s (f) Trailing edge of slug at $t + 0.35$ s

Figure 4. Transition of stratified flow to the slug flow during the geyser in the window of $x = -0.75$ m to $x = -0.85$ m. Progress of the slug in the horizontal pipe is shown in the sequence of images chronologically.

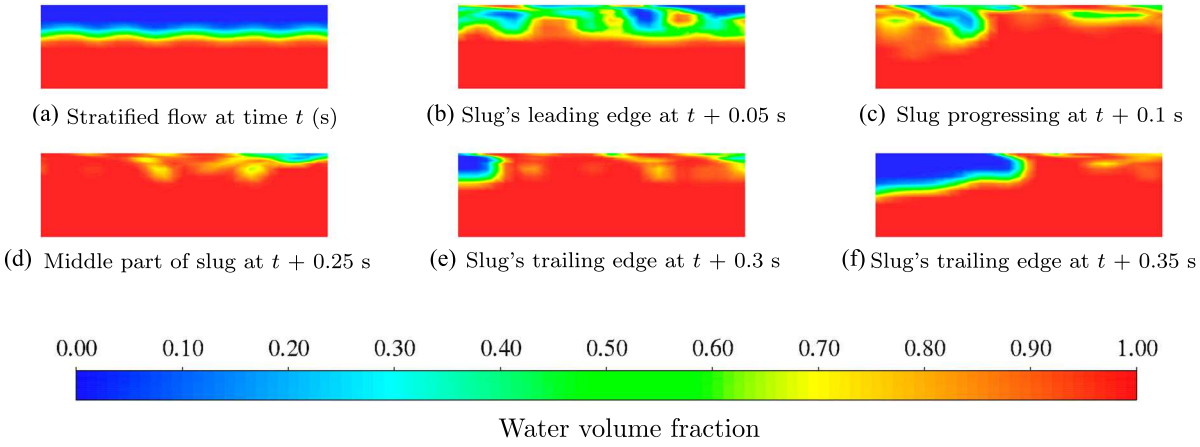

(a) Stratified flow at time t (s) (b) Slug's leading edge at $t + 0.05$ s (c) Slug progressing at $t + 0.1$ s

(d) Middle part of slug at $t + 0.25$ s (e) Slug's trailing edge at $t + 0.3$ s (f) Slug's trailing edge at $t + 0.35$ s

Figure 5. Prediction of slug in the window of $x = -0.75$ m to $x = -0.85$ m using coarse cutcell mesh.

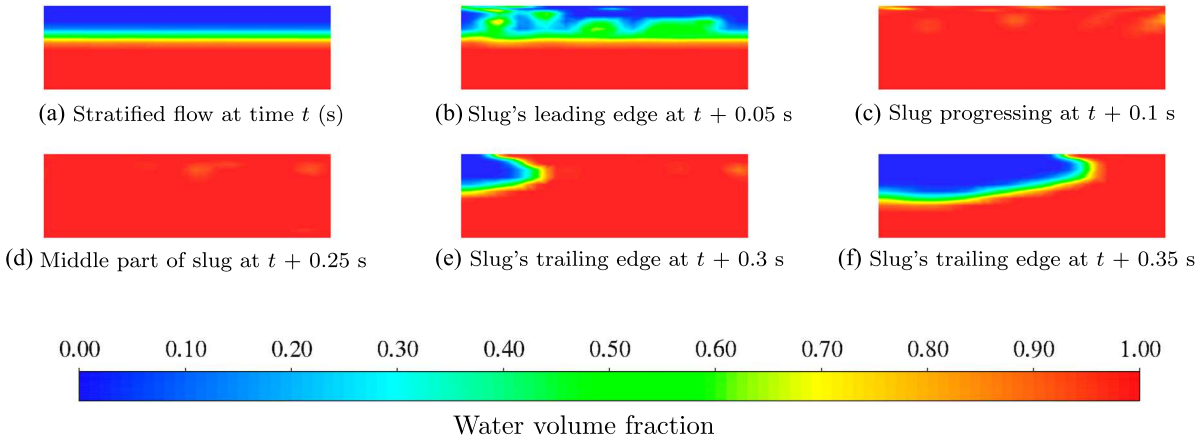

(a) Stratified flow at time t (s) (b) Slug's leading edge at $t + 0.05$ s (c) Slug progressing at $t + 0.1$ s

(d) Middle part of slug at $t + 0.25$ s (e) Slug's trailing edge at $t + 0.3$ s (f) Slug's trailing edge at $t + 0.35$ s

Figure 6. Prediction of slug in the window of $x = -0.75$ m to $x = -0.85$ m using medium refined cutcell mesh.

Figure 4 shows the slug progression captured by a high-speed camera in the geyser experiment. Each section of the slug is depicted in the sequence of images. Initially, stratified flow transforms into slug flow due to rapid air movement during the geyser eruption. A comparison of Figure 4a, b with Figure 4e, f demonstrates that the leading edge of the slug moves much faster than its trailing edge. This indicates that the slugs keep growing longer as they progress downstream. All stages of the slug and its characteristics are compared with those produced through numerical simulations. Figures 5–7 exhibit excellent predictions of slug generation, with all characteristics matching the experiments. The interfaces are thicker in the coarse mesh and get thinner with refinement; however, this does not significantly impact the high-level unsteady fluid dynamics. The coarser and medium-refined mesh loosely captures the slug's leading edge, whereas the refined mesh successfully captures each stage of the slug movement. Therefore, the simulation result from a refined mesh is considered for detailed analysis and further comparison against experiments. The animation of the water volume fraction contour and experimental videos are available in Movie-1 (Video link).

The refined mesh is approximately ten times more computationally expensive than the coarser mesh. Additionally, the time step fluctuates around 5e−5 s and 5e−4 s for the refined and coarser mesh, respectively.

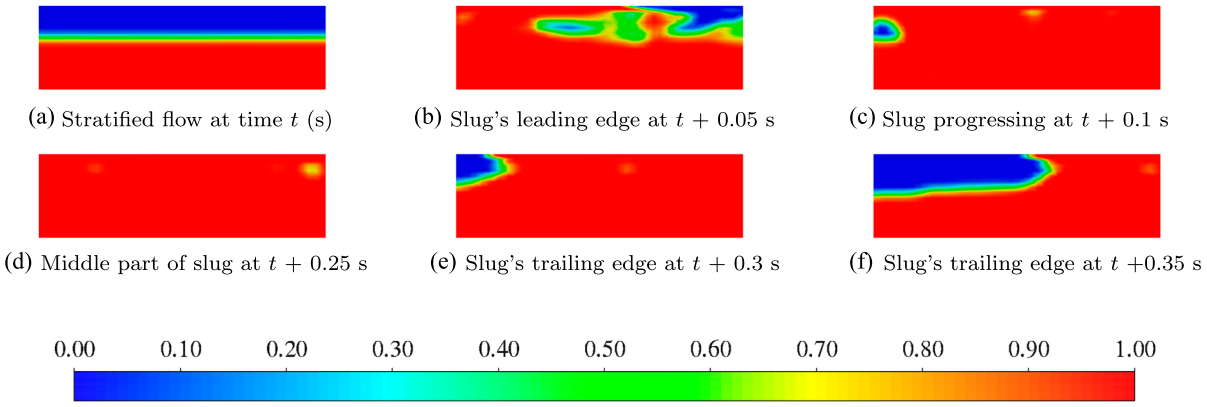

Figure 7. Prediction of slug in the window of $x = -0.75$ m to $x = -0.85$ m using refined cutcell mesh.

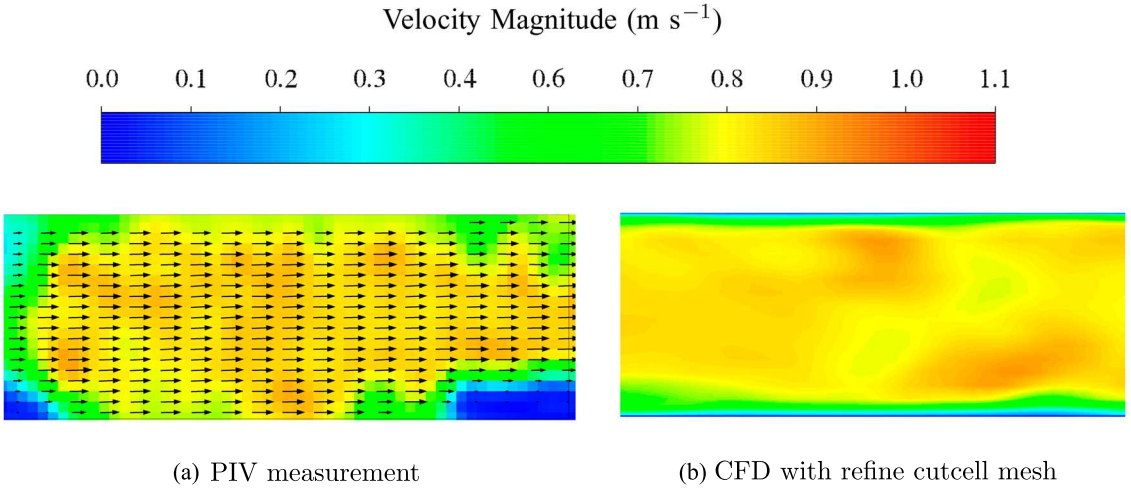

Figure 8. Comparison of slug's velocity predicted with CFD with refined cutcell mesh against the PIV measurement. The velocity magnitude is similar in both cases.

In the case of the coarser mesh, the diffused interface predicts a dilute mixture of air–water, which is uniformly distributed in the vertical pipe. Following this, the sharp interface cannot be recovered in the vertical pipe. Also, the coarser grid in the eruption region leads to significant errors in the prediction of eruption patterns.

5. Results and discussion

In this section, first, the geyser simulation with the refined cutcell mesh is discussed and compared with the experimental result. Second, using the established methodology, a geyser simulation with a trapped air pocket is presented.

The geyser simulation with the refined cutcell mesh exhibits similar dynamics as observed in the experiments. The air pocket arrives at the junction, rises in the vertical pipe, and produces an eruption of the air–water mixture. After one or two eruptions, the water fills the vertical pipe, pushing back the air pocket in the upstream direction in a horizontal pipe. This entire process is called one geyser cycle, which can have one or more eruptions depending on the operating conditions. Just before the first eruption or spillage, the drop in hydrostatic pressure in the vertical pipe results in the rapid suction of the air pocket. The fast-moving air pocket produces slugs in the horizontal pipe, as observed in both experiments and numerical simulations.

Figure 8 compares the numerically predicted slug's velocity against the PIV measurements. The corresponding slug images are shown in Figures 4d and 7d. The magnitudes of the velocities are almost uniform in both cases, approximately 0.8 to 0.9 (m s^{-1}). This further validates the numerical capabilities to predict geyser dynamics. Since the air was not seeded, only the water velocity was measured using PIV.

Figure 9 compares the static pressure numerically predicted at station P1 ($y = 0$ m) and P2 ($y = 0.3$ m) against the experimental measurement. The pressure fluctuations at station P1 are accurately predicted in magnitude and frequency, except at a few locations where discrepancies occur due to experimental uncertainties such as instrument errors, boundary conditions, pipe roughness and ambient conditions. These discrepancies also arise because of the finite size of the air tank, leading to minor pressure drops ($< 2\%$) at the

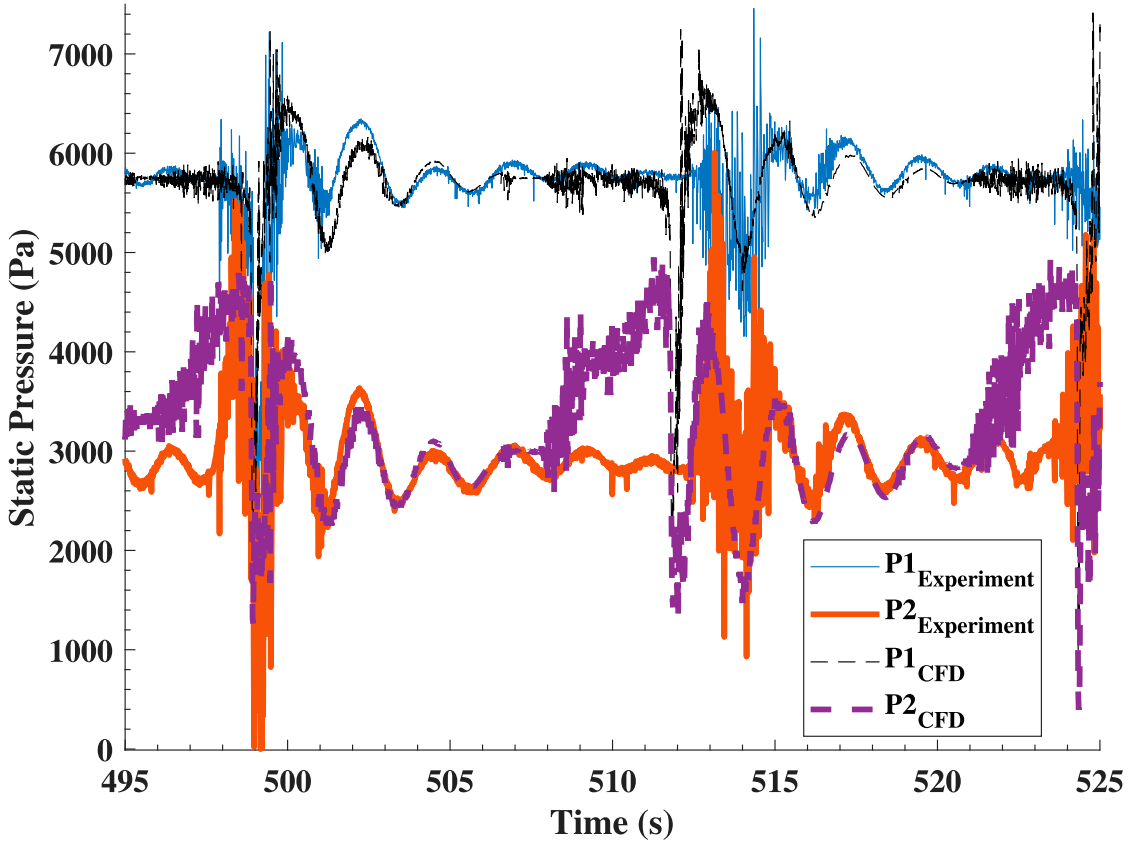

Figure 9. Numerically predicted static pressure compared against experiments.

air inlet during geyser eruptions. For station P2, numerical simulations overpredict the formation of residual bubbles and show a smooth pressure increment, which is not observed in the experiments. In other words, in experiments, air dominates the vertical pipe as soon as it arrives. The trapped air bubble can experience acceleration larger than gravity in the vertical pipe (Baumbach et al., 2005). In contrast, complex air–water mixing is first observed in the CFD, gradually pushing liquid upwards and forming a geyser. However, the CFD accurately predicted the eruption magnitude and post-eruption oscillations of water. Figure 9 describes the geyser process as follows:

(1) At time 508 s, the air pocket enters the vertical pipe and lifts the water column which results in a pressure rise at station P2 while the pressure at station P1 remains constant.
(2) In the experiment the air enters at time 512 s and takes approximately 1 s to produce spillage, whereas in the CFD simulation, it takes more than 3 s.
(3) The sharp drop in pressure at stations P1 and P2 at time 511 s is due to spillage which removes a large part of the water from the vertical pipe and exposes the pressurized air pocket to the near ambient pressure. In the experiment, station P2 showed a larger drop compared to P1 at time 513 s. This shows the rate of change of pressure (dp/dt) increases with height.
(4) The pressure drop propels the air–water mixture in the vertical pipe to produce one or two eruptions which further reduces the pressure at stations P1 and P2.
(5) Meanwhile the accelerated air produces one or two slugs in the horizontal pipe as shown in Figures 4 and 7.
(6) These slugs propagate towards the junction collecting more and more water until they climb the vertical pipe recovering hydrostatic pressure at stations P1 and P2.
(7) The recovery process overshoots the equilibrium position and produces an underdamped harmonic oscillation of a period of approximately 2 s.
(8) The overshoot in the hydrostatic pressure cuts air supply to the vertical pipe, pushing air in the upstream direction, and the system tends to move towards the original equilibrium state.
(9) Once the equilibrium is reached, the air pocket moves towards the vertical pipe and repeats the same process. The total time taken in the entire process is approximately 9.5 s.

Figure 10f–j show the eruption structure simulated using the refined cut cell mesh and visualized using an iso-surface of volume fraction at 0.5. The eruption height and width are similar to those observed in the experiments, as shown in Figure 10. The eruption begins with the initial water spillage, which rises higher as the water column keeps moving upward.

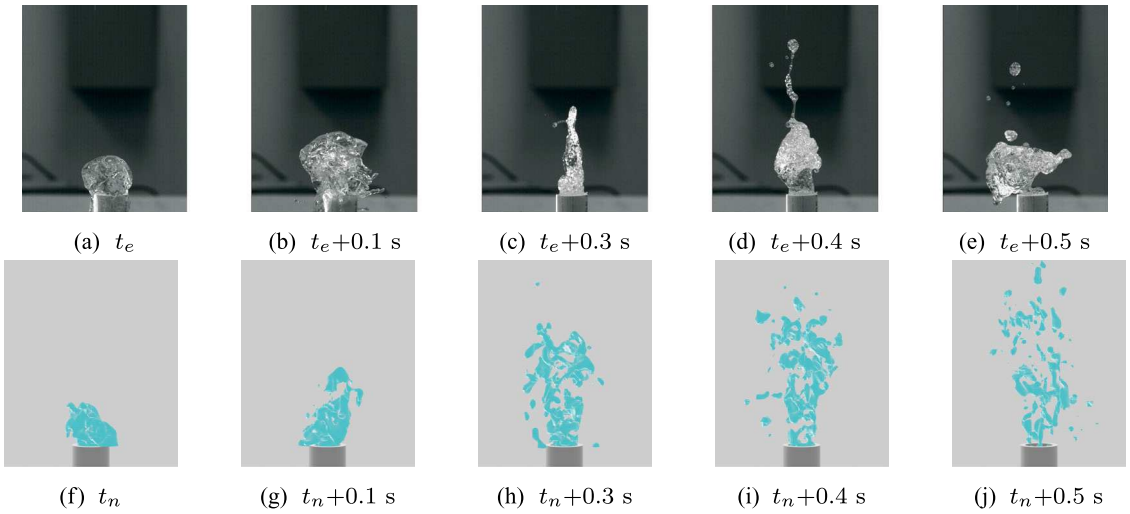

Figure 10. Numerically predicted eruption pattern compared against experiments. t_e and t_n are the experimental and numerical reference time at the beginning of the eruption.

The water column is followed by an air pocket and then a slug, which breaks the interface and pushes the air–water mixture further upward and in lateral directions. Depending on the number of slugs generated in the vertical pipe, a series of eruptions can be observed for one geyser cycle. Since this is a small-scale set-up, only one or two slugs are observed in a given geyser cycle. The slugs originate in the horizontal pipe and enter the vertical pipe at high velocity. However, these slugs are richer in water due to small-scale effects, and hence, if the slugs are large, they quickly lose momentum in the vertical pipe, preventing further eruptions. The slug sizes and frequency depend on the ratio of total to dynamic pressure; the higher the ratio, the greater the possibilities of slug production, as shown by Mahyawansi, Lin, et al. (2022).

Figure 11 compares the temporal history of geyser height in experiments and simulations. The numerical methodology accurately predicted various eruption features such as geyser duration, maximum eruption height, and eruption sequences. However, the numerical results are more continuous than the experimental results, probably because the simulation overestimates air–water mixing prior to eruptions, which results in a smoother eruption profile.

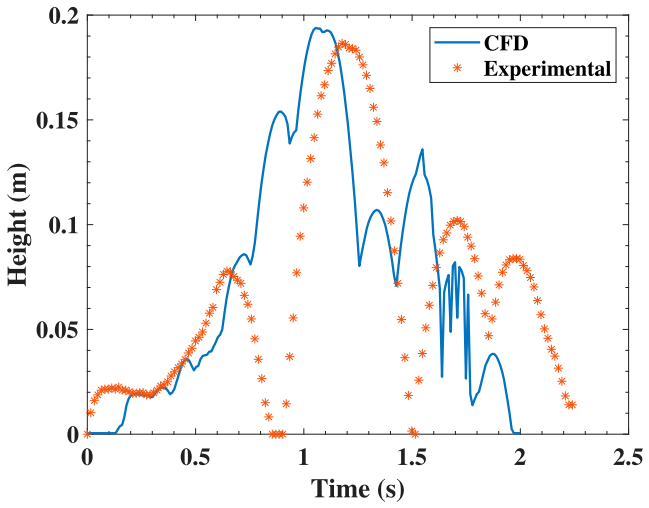

Figure 11. Temporal history of geyser height in one geyser cycle in experiment and simulation.

5.1. Application of CFD methodology for simulating geyser with large trapped air pocket

The established CFD methodology is tested on the longer set-up with a given amount of trapped air (0.002774 m^3). Figure 12 shows the extended set-up without an air-inlet boundary; the upstream and downstream ends of the pipe are extended by 10 m and 5 m, respectively. The boundary conditions are intact except at the inlet and outlet, where a slight adjustment in the pressure head was required due to added pipe loss. Initially, the flow is allowed to reach a steady state, i.e. an average velocity of 0.06 m s^{-1}, and the water level in the vertical pipe is 0.5842 m from the pipe centre. Once the flow reaches a steady state, trapped air is introduced by patching the volume fraction variable in the upstream pipe. The total length of the air volume is 10.95 m, which spans from $x = -11$ m to $x = -0.05$ m, where the origin is at the pipe junction. The Courant number was initially kept at 2 for the first two seconds, then increased to 5. The simulation time-step fluctuates around 5e−5 s. This set-up allows flow-driven insertion of air into the vertical pipe, which closely resembles the hypothesized scenario in the storm sewer geyser. The local hydrostatic pressure in the horizontal pipe governs the air pocket pressure. This is a major difference from the previous simulation, where air pressure was controlled by the air tank or air-inlet boundary.

Figure 13 shows the variation in static pressure at all six stations during the interaction of the air pocket with the vertical pipe. Initially, steady pressure at all stations

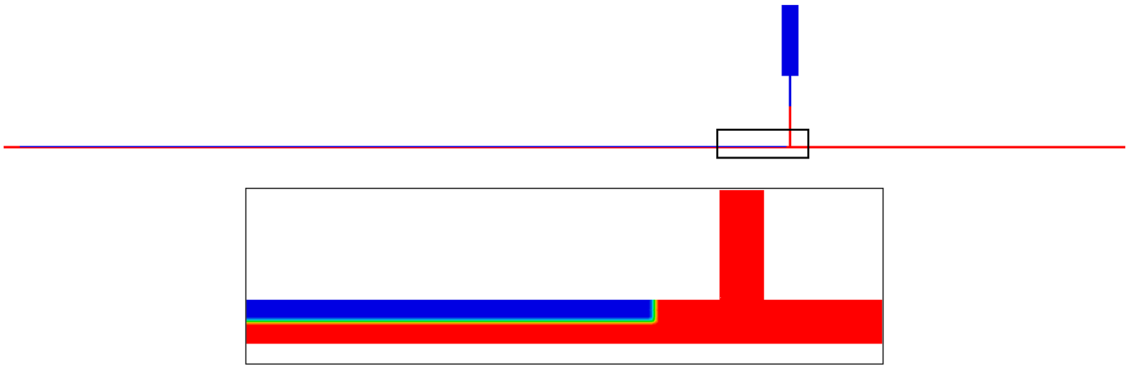

Figure 12. Set-up for geyser simulation with trapped air of volume 0.002774 m^3. The bottom image is zoomed view of the top image in the region enclosed by a black rectangular box.

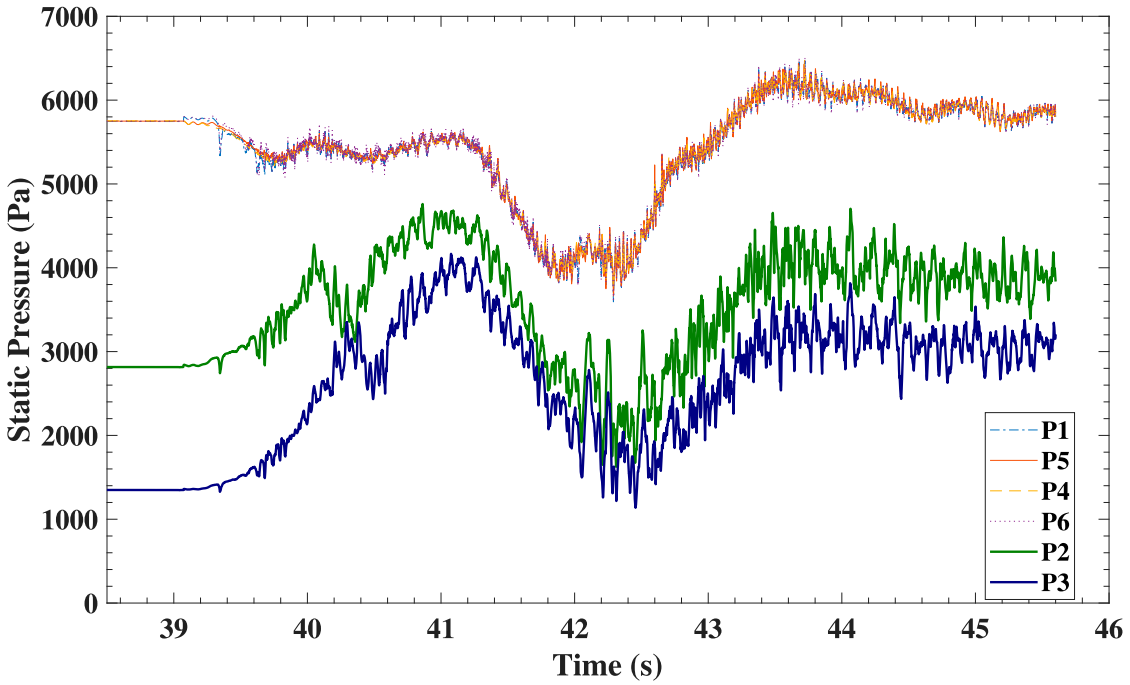

Figure 13. Numerically predicted static pressure during geyser by a fixed quantity of trapped air.

experiences significant changes in magnitude. The percentage change in pressure is inversely proportional to the initial hydrostatic pressure. Most importantly, the pressure variation at all stations in the horizontal pipe varies uniformly for low-frequency (< 1 Hz) perturbations. This indicates that the static pressure primarily varies in time and the y-direction , i.e. the gradient $\partial p/\partial x$ is relatively small for the entire geyser process.

Figure 14 shows the velocity magnitude recorded at all six stations. For stations P2 and P3, the velocity magnitude increases linearly and then transforms into violently fluctuating signals. The maximum velocities are observed between 42 to 44 s, where the pressure oscillations turn aggressive at higher frequencies (> 1 Hz). Figure 15 shows the stages of air–water interactions for the entire geyser process, visualized using the contour of water volume fraction. The observations from plots and contours of a simulated geyser process are summarized as follows:

(1) At 39.642 s, the air pocket starts entering the vertical pipe lifting the water in its path.
(2) The pressure at stations P2 and P3 gradually increases in a synchronized manner due to the rise of the water level. A small fraction of the lifted water keeps falling back through a thin liquid film between air and pipe wall.
(3) At approximately 40 s, the pressure at P2 drops due to the arrival of an air pocket, which is also seen at P3 after the delay of 0.3 s.
(4) At this point, the mixing of falling water and air produces slugs in the vertical pipe and moves upwards.
(5) At 41.2 s, the lifted water spills from the top of the pipe and results in dramatic pressure drops at all stations.
(6) This results in acceleration of the slug, enabling it to rush out from the pipe and continue to move upwards in the atmosphere till it loses momentum.

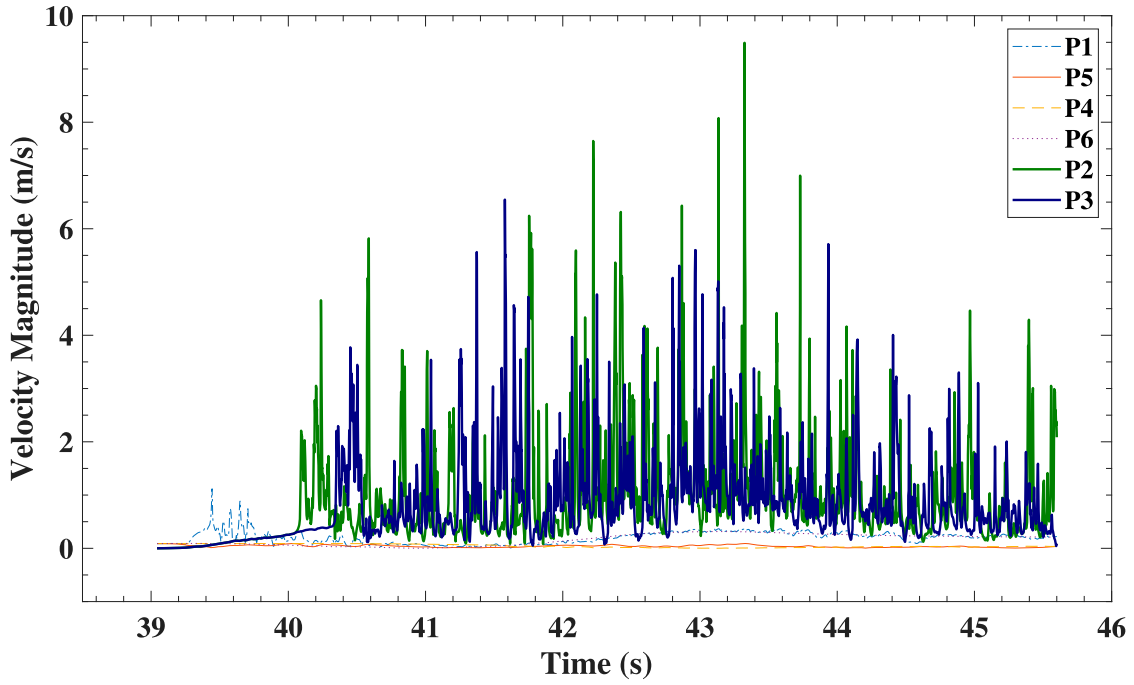

Figure 14. Numerically predicted velocity magnitude during a geyser produced by a fixed quantity of trapped air.

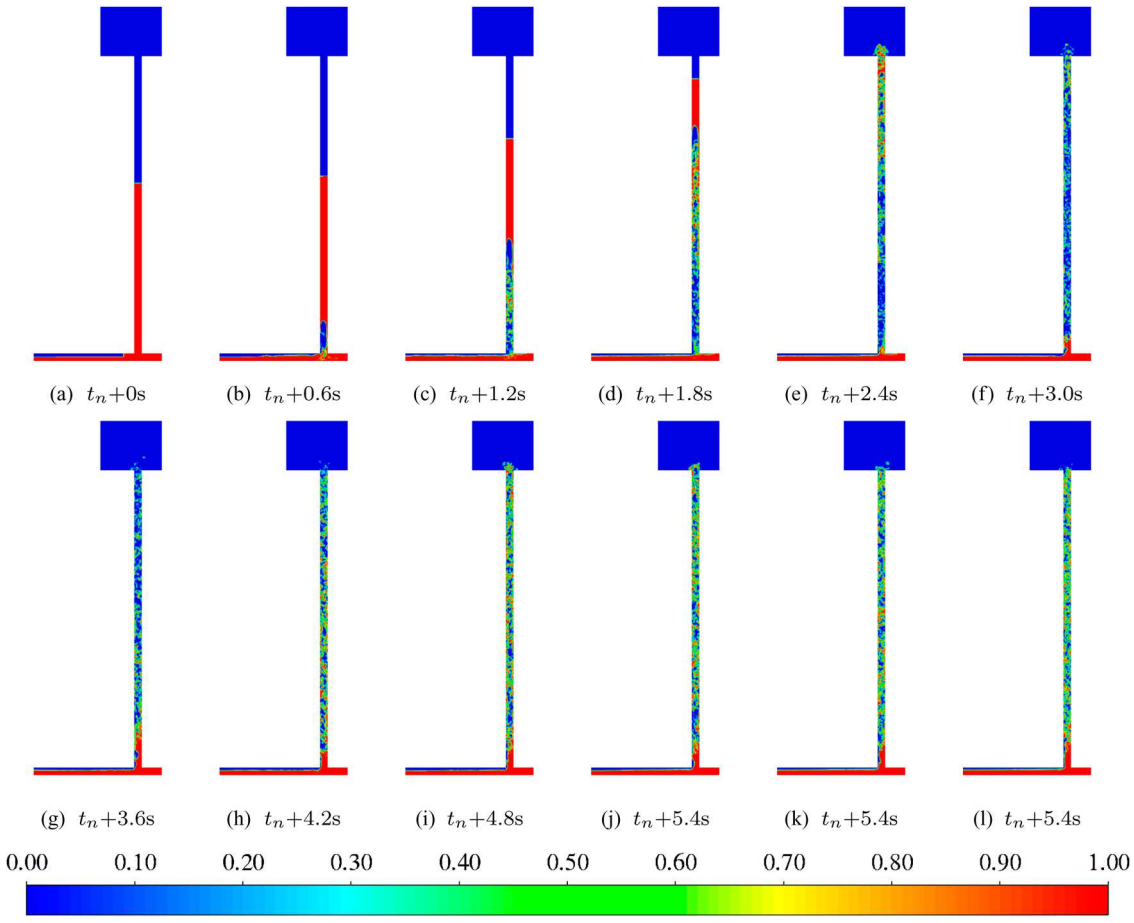

Figure 15. Numerically predicted volume fraction of water (designated by red colour) in an extended pipe system with the initial water level at 0.584 m from the junction centre, $t_n = 39.04$ s

(7) The drop in static pressure in the entire vertical pipe results in the suction of water from the horizontal pipe.
(8) The air and water both struggle to claim the vertical pipe, due to which the air dominates the left side bottom of the vertical pipe and the water on the right side.
(9) This produces large shear at the interface, resulting in an air–water mixture in the form of small slugs.

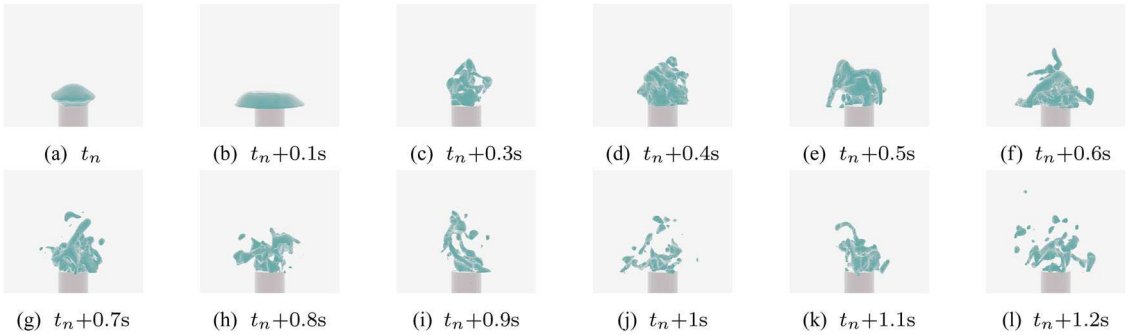

Figure 16. Numerically predicted eruption pattern visualized by the iso-surface of 0.5 water volume fraction where $t_n = 41.642$ s.

(10) These small slugs keep moving upwards at high velocity and produce subsequent eruptions, which can be seen in the pressure and velocity plot as large amplitude fluctuations.

Figure 16 shows the eruption pattern observed in the simulation. The ejected water is tracked by the iso-surface of the water volume fraction at 0.5. The eruption height is lower than in the previous simulation, where air-inlet pressure was fixed. In this case, the eruption is primarily driven by the dynamics of the vertical pipe. The observation is summarized below.

(1) The air–water mixture accelerates upwards and achieves a height of 0.05 to 0.07 m above the ground.
(2) The geyser process lasts longer than the previous set-up and it consists of a large number of eruptions.
(3) The eruptions are driven by the formation of slugs or the breaking of the water columns by the rapidly rising air.
(4) The volume fraction of water in the erupted mixture decreases as the geyser progresses.

The summary of the geyser process is shown in the animation video in Movie-2 (video link). A geyser is a chain of eruptions of a mixture with high concentrations of air; however, in the presented small-scale study, the experiments and numerical simulations have relatively low concentrations of air which limits the geyser severity. Major findings of the geyser process from its simulation due to a trapped air pocket are as follows:

(1) The trapped air pocket allows smooth injection of air in the vertical pipe.
(2) The air pocket maintains pressure equilibrium with the water and does not propel it in the horizontal pipe.
(3) There is no slug generation in the horizontal pipe which results in a continuous air supply to the vertical pipe.
(4) The air–water mixing takes place in a vertical pipe which produces a churn-slug flow.

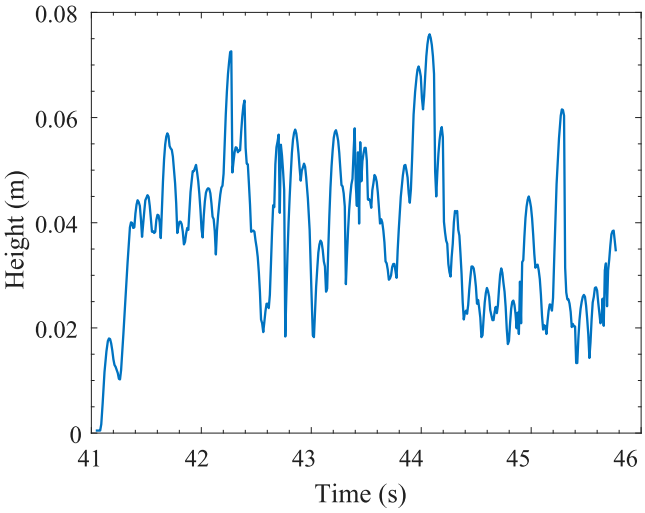

Figure 17. Temporal history of geyser height due to finite trapped air pocket.

(5) These churn-slug mixtures in the vertical pipe erupt in a sequence, creating a long-lasting geyser as shown in Figure 17, with the eruption height reaching approximately 2.7 times the pipe diameter.
(6) The temporal history of geyser height shows the eruption progression which gradually increases with time and fluctuates between 0.02 to 0.07 m.
(7) Small-scale geysers have dominant surface tension effects on the atomization of the air–water interface that limit mixing in the vertical pipe and hence, produce lower momentum eruptions.

Small-scale geysers have dominant surface tension effects on the atomization of the air–water interface that limit mixing in the vertical pipe and hence, produce lower momentum eruptions. A similar study with a larger pipe diameter may give a relatively higher eruption height. This will be investigated in the future.

6. Conclusion

A numerical methodology was explored to simulate storm sewer geysers using a VOF multiphase model with anti-diffusion and LES turbulence model. A

lab-scale set-up is utilized to study a geyser-like process by supplying air at a constant pressure. Smaller set-ups are easier to simulate; therefore, few parameters are varied including grid types (polyhedral and cutcell) and refinement levels. The modelling technique is validated against experimental results, which encompass interface locations, slug velocity, pressure fluctuations, and eruption patterns.

The expensive polyhedral mesh is found to be incapable of accurately predicting the geyser process, whereas simulations using a fairly affordable cutcell mesh successfully capture all the essential geyser features. The slug characteristics, such as shape and length in the horizontal pipe, are accurately predicted. Additionally, the predictions of pressure oscillations at the junction and in the vertical pipe agree with experimental data. However, the simulations tend to over-predict the mixing of air and water, leading to slower rise of the liquid column. The PIV technique is used to measure slug velocity in the horizontal pipe; however, the study is limited to the middle part of the slug where the flow is unmixed to avoid refractions due to bubbles. PIV measurements validate the slug velocity predicted by the simulations.

The geyser process, from spillage to fully developed eruption, is found to closely match the experimental high-speed videography. The over-prediction of mixture in the vertical pipe likely leads to a continuous eruption process in the simulation, while the experiment demonstrates a discontinuous eruption progression. Nevertheless, the simulation yielded promising results in predicting all the important geyser features listed above.

The established methodology is applied to simulate a geyser with a trapped air pocket in the extended CFD domain. The eruption structures are found to be similar to those of an actual storm sewer geyser in terms of the progression of velocity and pressure oscillations. In the geyser with the trapped air pocket, slugs are not produced in the horizontal pipe; instead, a combination of churn and slug flow is observed in a vertical pipe, contributing to the eruptions. However, the current operating conditions are not sufficient to generate violent geysers. Therefore, additional studies are required under different operating conditions with a set-up that allows pressure oscillations to grow further, potentially resulting in violent eruptions.

Notation

α_1	air volume fraction (–)
α_2	water volume fraction (–)
Δ	grid scale (m)
∇	gradient function (m^{-1})
ρ_1	air density ($kg\,m^{-3}$)
ρ_2	water density ($kg\,m^{-3}$)
ρ	phase averaged density ($kg\,m^{-3}$)
μ_1	molecular viscosity of air (Pa s)
μ_2	molecular viscosity of water (Pa s)
μ	phase averaged molecular viscosity (Pa s)
μ_t	eddy viscosity (Pa s)
$\boldsymbol{\tau_{ij}}$	Subgrid stress tensor (Pa)
C_s	Smagorinsky constant
d	distance from the nearest wall (m)
E	total energy of the mixture per unit mass ($J\,kg^{-1}$)
F	surface tension force ($N\,m^{-3}$)
g	acceleration due to gravity ($m\,s^{-2}$)
k	von Kármán constant
k_{eff}	effective thermal conductivity ($W\,m^{-1}\,K^{-1}$)
L_s	mixing length (m)
p	pressure (Pa)
$\bar{\mathbf{S}}_{\mathbf{ij}}$	rate-of-strain tensor of resolved scales (s^{-1})
T	temperature (K)
t	time (s)
V	velocity ($m\,s^{-1}$)
x	x-coordinate (m)
y	y-coordinate (m)

Acknowledgments

The author would like to acknowledge the late Prof. Cheng-Xian Lin for his support and guidance in this work. The author would also like to acknowledge Ms Diana Rivero for reviewing the readability of the paper.

Disclosure statement

No potential conflict of interest was reported by the author(s).

Funding

The authors gratefully acknowledge the financial support of the National Science Foundation (NSF) under grant number 1928850. The views expressed are solely those of the authors. NSF does not endorse any products or commercial services mentioned.

ORCID

Pratik Mahyawansi http://orcid.org/0000-0002-3457-9650

References

Ansys (2022). Ansys® Academic Research Fluent, Release 22.2.0.

Baumbach, V., Hopfinger, E. J., & Cartellier, A. (2005). The transient behaviour of a large bubble in a vertical tube. *Journal of Fluid Mechanics*, *524*, 131–142. https://doi.org/10.1017/S0022112004001995

Blender-Online-Community (2020). *Blender – a 3D modelling and rendering package* [Computer software manual]. Stichting Blender Foundation.

Guo, Q., & Song, C. C. (1990). Surging in urban storm drainage systems. *Journal of Hydraulic Engineering*, *116*(12), 1523–1537. https://doi.org/10.1061/(ASCE)0733-9429(1990)116:12(1523)

Gupta, V. K., Khan, M., & Punekar, H. (2015). Development and application of interfacial anti-diffusion and poor

mesh numerics treatments for free surface flows. In *2015 IEEE 22nd international conference on high performance computing workshops* (pp. 12–18).

Hirt, C., & Nichols, B. (1981). Volume of fluid (VOF) method for the dynamics of free boundaries. *Journal of Computational Physics*, *39*(1), 201–225. https://doi.org/10.1016/0021-9991(81)90145-5

Lakehal, D. (2018). Status and future developments of Large-Eddy simulation of turbulent multi-fluid flows (LEIS and LESS). *International Journal of Multiphase Flow*, *104*, 322–337. https://doi.org/10.1016/j.ijmultiphaseflow.2018.02.018

Lakehal, D., Fulgosi, M., Yadigaroglu, G., & Banerjee, S. (2003). Direct numerical simulation of turbulent heat transfer across a mobile, sheared gas-liquid interface. *Journal of Heat Transfer*, *125*(6), 1129–1139. https://doi.org/10.1115/1.1621891

Leon, A. S. (2019). Mechanisms that lead to violent geysers in vertical shafts. *Journal of Hydraulic Research*, *57*(3), 295–306. https://doi.org/10.1080/00221686.2018.1459895

Mahyawansi, P., Lin, C. X., & Leon, A. S. (2022). Understanding the influence of pressure disturbance on the transition of stratified to slug flow. In *7th thermal and fluids engineering conference (TFEC)*.

Mahyawansi, P., Zange, S. R., Lin, C. X., & Leon, A. S. (2022). An affordable PIV technique for water using potato starch with diode laser and smartphones. In *World environmental and water resources congress 2022* (pp. 390–399).

Mortazavi, M., Le Chenadec, V., Moin, P., & Mani, A. (2016). Direct numerical simulation of a turbulent hydraulic jump: Turbulence statistics and air entrainment. *Journal of Fluid Mechanics*, *797*, 60–94. https://doi.org/10.1017/jfm.2016.230

Muller, K. Z., Wang, J., & Vasconcelos, J. G. (2017). Water displacement in shafts and geysering created by uncontrolled air pocket releases. *Journal of Hydraulic Engineering*, *143*(10), Article 04017043. https://doi.org/10.1061/(ASCE)HY.1943-7900.0001362

Pavlidis, D., Xie, Z., Percival, J. R., Gomes, J. L., Pain, C. C., & Matar, O. K. (2014). Two-and three-phase horizontal slug flow simulations using an interface-capturing compositional approach. *International Journal of Multiphase Flow*, *67*, 85–91. https://doi.org/10.1016/j.ijmultiphaseflow.2014.07.007

Qian, Y., Zhu, D. Z., Liu, L., Shao, W., Edwini-Bonsu, S., & Zhou, F. (2020). Numerical and experimental study on mitigation of storm geysers in Edmonton, Alberta, Canada. *Journal of Hydraulic Engineering*, *146*(3), Article 04019069. https://doi.org/10.1061/(ASCE)HY.1943-7900.0001684

So, K., Hu, X., & Adams, N. A. (2012). Anti-diffusion interface sharpening technique for two-phase compressible flow simulations. *Journal of Computational Physics*, *231*(11), 4304–4323. https://doi.org/10.1016/j.jcp.2012.02.013

Thielicke, W., & Sonntag, R. (2021). Particle image velocimetry for MATLAB: Accuracy and enhanced algorithms in PIVlab. *Journal of Open Research Software*, *9*. https://doi.org/10.5334/jors.334

Vasconcelos, J. G., & Wright, S. J. (2006). Mechanisms for air pocket entrapment in stormwater storage tunnels. In *World environmental and water resource congress 2006: Examining the confluence of environmental and water concerns* (pp. 1–10).

Vasconcelos, J. G., & S. J. Wright (2011). Geysering generated by large air pockets released through water-filled ventilation shafts. *Journal of Hydraulic Engineering*, *137*(5), 543–555. https://doi.org/10.1061/(ASCE)HY.1943-7900.0000332

Wright, S. J., Lewis, J. W., & Vasconcelos, J. G. (2011). Physical processes resulting in geysers in rapidly filling storm-water tunnels. *Journal of Irrigation and Drainage Engineering*, *137*(3), 199–202. https://doi.org/10.1061/(ASCE)IR.1943-4774.0000176

Zanje, S. R., Mahyawansi, P., Leon, A. S., & Lin, C. X. (2022). CFD modeling of storm sewer geysers in partially filled dropshafts. In *World environmental and water resources congress 2022* (pp. 1187–1195).